Clim Dyn
DOI 10.1007/s00382-013-1884-8

Diagnosis and testing of low-level cloud parameterizations for the NCEP/GFS model using satellite and ground-based measurements

Hyelim Yoo · Zhanqing Li · Yu-Tai Hou · Steve Lord · Fuzhong Weng · Howard W. Barker

Received: 8 October 2012 / Accepted: 15 July 2013

Abstract The objective of this study is to investigate the quality of clouds simulated by the National Centers for Environmental Prediction global forecast system (GFS) model and to examine the causes for some systematic errors seen in the simulations through use of satellite and ground-based measurements. In general, clouds simulated by the GFS model had similar spatial patterns and seasonal trends as those retrieved from passive and active satellite sensors, but large systematic biases exist for certain cloud regimes especially underestimation of low-level marine stratocumulus clouds in the eastern Pacific and Atlantic oceans. This led to the overestimation (underestimation) of outgoing longwave (shortwave) fluxes at the top-of-atmosphere. While temperature profiles from the GFS model were comparable to those obtained from different observational sources, the GFS model overestimated the relative humidity field in the upper and lower troposphere. The cloud condensed water mixing ratio, which is a key input variable in the current GFS cloud scheme, was largely underestimated due presumably to excessive removal of cloud condensate water through strong turbulent diffusion and/or an improper boundary layer scheme. To circumvent the problem associated with modeled cloud mixing ratios, we tested an alternative cloud parameterization scheme that requires inputs of atmospheric dynamic and thermodynamic variables. Much closer agreements were reached in cloud amounts, especially for marine stratocumulus clouds. We also evaluate the impact of cloud overlap on cloud fraction by applying a linear combination of maximum and random overlap assumptions with a de-correlation length determined from satellite products. Significantly better improvements were found for high-level clouds than for low-level clouds, due to differences in the dominant cloud geometry between these two distinct cloud types.

Keywords Marine stratocumulus cloud · NCEP global forecast system · Cloud parameterization scheme · Cloud overlap

This paper is a contribution to the Topical Collection on Climate Forecast System Version 2 (CFSv2). CFSv2 is a coupled global climate model and was implemented by National Centers for Environmental Prediction (NCEP) in seasonal forecasting operations in March 2011. This Topical Collection is coordinated by Jin Huang, Arun Kumar, Jim Kinter and Annarita Mariotti.

H. Yoo · Z. Li
Dept of Atmospheric and Oceanic Science,
University of Maryland, College Park, MD 20740, USA

Z. Li (✉)
State Key Laboratory of Earth Surface Processes and Resource Ecology, College of Global Change and Earth System Sciences, Beijing Normal University, Beijing 100875, China
e-mail: zli@atmos.umd.edu

Y.-T. Hou · S. Lord
Environmental Modeling Center, NCEP/NWS/NOAA,
5830 University Research Court, College Park, MD 20740, USA

F. Weng
STAR/NESDIS, NOAA, 5830 University Research Court,
College Park, MD 20740, USA

H. W. Barker
Environment Canada, Toronto, Canada

1 Introduction

Clouds play key roles in Earth's climate system by regulating Earth's energy budget and water cycle (Morcrette and Fouquart 1986; Tian and Curry 1989; Rossow and Zhang 1995; Barker et al. 1999; Collins 2001). Despite

Published online: 31 July 2013

their significance, the representation of clouds in global climate and weather models has been problematic due to an incomplete knowledge of underlying physical processes (Stephens 2005) which also vary considerably both vertically and horizontally (Rossow et al. 1989). Cloud representations in models are a critical source of uncertainty in predictions of climate change (Randall et al. 2007; Wielicki et al. 1995; Houghton 2001).

Global climatologies of occurrence frequencies of low clouds were compiled over the eastern tropical oceans from synoptic surface cloud observations (Norris 1998). Studies have shown that many general circulation models (GCMs) have difficulty in representing low cloud distributions (Ma et al. 1996; Hannay et al. 2009). This is also a problem for fully-coupled climate system models (Dai and Trenberth 2004; Mechoso et al. 1995), weather forecasting models (Ahlgrimm and Köhler 2010) and regional climate models (Xie et al. 2007). This inability of simulating the marine stratocumulus cloud decks is one of the most significant sources of errors associated with cloud feedback processes (Bony and Dufresne 2005; Randall et al. 2007) and it can have a large effect on temperature forecasts (Boutle and Abel 2012) and shortwave irradiance budgets at the surface (Ahlgrimm and Forbes 2012). Underestimation of stratocumulus clouds over eastern subtropical oceans has also been a long-standing problem in the National Centers for Environmental Prediction (NCEP) global forecast system (GFS) model (Sun et al. 2010). Marine stratocumulus and low clouds over the oceans are known to have a net radiative cooling effect on the global energy budget by reflecting incoming solar radiation (Hartmann et al. 1992); they have little impact on the longwave radiation budget. Under-prediction of such clouds by ocean–atmosphere coupled models led to ocean temperatures off the coast of Peru that were too warm (de Szoeke et al. 2006). Improving the representation of marine stratocumulus clouds in global climate and weather forecasting models is highly desirable (Boutle and Morcrette 2010).

As more observational data become available, they are being increasingly employed in validating GCM-modeled clouds. The International Satellite Cloud Climatology Project (ISCCP) (Rossow and Schiffer 1999) dataset is among the most widely used set of satellite products (Webb et al. 2001; Zhang et al. 2005). Evaluations revealed that GCMs tend to produce less low-level clouds and much less mid-level clouds than the ISCCP product. It is worth noting that satellite cloud products suffer from significant uncertainties in the detection of multi-layered clouds. Knowledge about multi-layered clouds is important for climate-change studies because observations from ships (Warren et al. 1985), airborne lidar measurements (Platt et al. 1994; Clothiaux et al. 2000), and surface-based radar (Mace and Benson-Troth 2002) have detected the frequent occurrence of overlapped clouds. For satellite retrievals using a few channels from passive sensors, cirrus overlapping low-level liquid clouds tends to be misclassified as single-layer of mid-level clouds. This shortcoming can be greatly alleviated by taking advantage of multi-channel measurements from the Moderate Resolution Imaging Spectroradiometer (MODIS; Chang and Li 2005a, b). An algorithm developed by Chang and Li (referred to as the CL algorithm) can detect and retrieve the optical properties of low clouds below thin high clouds. The active sensors on CloudSat and Cloud-Aerosol Lidar and Infrared Pathfinder Satellite Observations (CALIPSO) satellites provide more direct and reliable information about cloud vertical profiles (Stephens et al. 2002; Mace et al. 2009).

In an earlier study (Yoo and Li 2012), extensive comparisons were made between GFS-modeled and satellite-retrieved cloud variables including cloud fraction, cloud optical depth, liquid and ice water paths, and the frequencies of multi-layer clouds on a global scale. Overall, their gross features match reasonably well in terms of locations and spatial patterns, although large discrepancies exist in their magnitudes. A drastic underestimation of low clouds over the eastern tropical oceans by the GFS model stood out as the most outstanding problem. This study aims at exploring the potential causes for this discrepancy through close-up investigations of the input variables and cloud parameterization schemes for determining cloud fraction and cloud overlap.

Marine stratocumulus clouds over the eastern tropical oceans are the main focus of the study. They are observed from space by active and passive satellite sensors. Model simulated temperature and relative humidity profiles are compared against retrievals from the atmospheric infrared sounder (AIRS) and ground-based measurements. The evaluation of atmospheric environmental variables allows for the investigation of whether discrepancies between the model and observations result from model input parameter deficiencies and/or cloud parameterization scheme deficiencies.

The manuscript is organized as follows. Section 2 describes the observational datasets used in this study. A brief description of the GFS model, global distributions of low-level cloud fraction and the radiation budget from observations and the GFS model, as well as comparisons of GFS-generated vertical profiles of temperature and relative humidity fields with observations are given in Sect. 3. Section 4 presents results from an application of the alternative cloud parameterization scheme to the GFS model. Characteristics of changes in cloud fraction due to the application of different cloud overlap assumptions are described in Sect. 5. Finally, Sect. 6 presents the main findings and a summary of this work.

2 Observational datasets

Atmospheric environmental variables from both the AIRS sensor onboard the Aqua satellite and a ground-based instrument located at the Southern Great Plains (SGP) site are used in this study. Cloud fractions are retrieved from the CL algorithm using MODIS data from the Aqua satellite platform and are also obtained from space-borne active sensors. These datasets are invaluable tools to use for monitoring clouds and changes in atmospheric temperature on a global scale and for assessing the accuracy of weather forecast models. Daily data in July 2007 and July 2008 are used in this study.

2.1 AIRS-space-borne atmospheric profile data

The AIRS sensor launched in May 2002 is the first high spectrally-resolving infrared sounder with near-global coverage on a daily basis (Aumann et al. 2003). It is deployed onboard the Aqua satellite in a Sun-synchronous orbit 705.3 km above the Earth's surface, with a southward crossing of the equator at 01:30 local time and a northward crossing of the equator at 13:30 local time. The AIRS measures temperature, water vapor, ozone profiles, and the presence of minor gases such as CH_4 and CO as well as other atmospheric properties at 2,378 infrared channels ranging from 15.38 to 3.74 μm (Chahine et al. 2006). Its spatial resolution is 13.5 km at nadir and the sensor is accompanied by two microwave sounders: the Advanced Microwave Sounding Unit-A (AMSU-A) and the Humidity Sounder for Brazil (HSB). These instruments are used to correct for cloud contamination in AIRS footprints. The AMSU-A footprint is about 45 km in diameter which contains 3 × 3 AIRS pixels. The final retrieval results have a horizontal resolution of 45 km (Aumann et al. 2003). Microwave-calibrated radiances are used to generate initial estimates of the temperature and moisture profiles because microwave data are not affected by most clouds. Calibrated AMSU-A brightness temperatures (Pagano et al. 2003) are utilized to derive atmospheric environmental profiles and cloud liquid water for microwave retrievals (Rosenkranz 2003; Susskind et al. 2003).

Based on previous studies (Susskind et al. 2006; Tobin et al. 2006; Walden et al. 2006), AIRS Level 2 data have an accuracy of ∼1 K root mean square (RMS) error in 1 km layers for temperature and have a 20 % RMS error in 2 km layers for water vapor amounts when compared to radiosonde data. Tobin et al. (2006) compared estimates of the atmospheric state at Aqua overpass times from three atmospheric radiation measurement (ARM) sites. They found that RMS differences for temperatures and water vapor profiles were around 0.3–0.7 K and 7–15 % at the Nauru site in the Tropical Western Pacific.

Divakarla et al. (2006) evaluated temperature and moisture profile retrievals from the AIRS data using more than 2 years of global radiosonde measurements (RAOB). The AIRS water vapor bias in 2 km layers is within 10 % compared to the reference (RAOB) below 400 mb, but it grows large negative above 400 mb because RAOB measurements have a moist bias above 400 mb. With respect to the temperature field, AIRS retrievals showed a ±0.7 K bias within the entire vertical column.

There are three different AIRS Level 2 version 5 standard daily products: AIRS infrared (IR) retrievals only, a combination of AMSU-A, AIRS IR and HSB retrievals, and a combination of AIRS IR and AMSU-A retrievals without HSB data. This study uses the latter dataset because AIRS IR-only retrieval uncertainties increase rapidly when cloud fractions exceed 80 % (Tobin et al. 2006) and HSB failed in February 2003.

2.2 MODIS-space-borne cloud data

The MODIS is the principal instrument onboard the polar-orbiting Terra and Aqua satellites and has 36 calibrated spectral channels ranging from 0.415 to 14.24 μm (Barnes et al. 1998). This sensor detects clouds and makes reliable retrievals of cloud properties (King et al. 2003; Ackerman et al. 1998; Menzel et al. 2002), such as cloud particle thermodynamic phase, cloud optical depth, cloud-top pressure and temperature, and effective particle radius using the MODIS CO_2 slicing method (Platnick et al. 2003).

Taking advantage of the multiple channels of the MODIS, the CL algorithm detects up to 27 % more low clouds over oceans and up to 29 % more clouds over land when compared to EOS/MODIS products (Chang and Li 2005b). This happens because the algorithm can identify low clouds overlapped by thin cirrus, this cloud scenario would be misidentified either as one-layer mid clouds if the conventional visible-infrared algorithm is employed or high thick clouds if a CO_2-slicing method is used. The merits of the new algorithm and products were demonstrated in a previous study comparing them to those derived from CloudSat/CALIPSO active sensors (Yoo and Li 2012). As such, this study uses cloud fractions from the CL algorithm and the MODIS Collection 5.1 cloud product.

2.3 CERES-space-borne Earth radiation budget data

The Clouds and the Earth's Radiant Energy System (CERES) instrument measures radiative fluxes at the top-of-atmosphere (TOA; Wielicki et al. 1995; Loeb et al. 2007). This sensor is onboard both Terra and Aqua satellites; only CERES data from the Aqua satellite are analyzed here. This study uses the Single Scanner Footprint

product which contains longwave/shortwave fluxes at the TOA and at the surface for clear and all-sky conditions on a daily basis. Outgoing longwave, shortwave, and net fluxes at the TOA are compared to corresponding output from the GFS model.

2.4 CloudSat and CALIPSO merged data

The CloudSat and CALIPSO satellites were launched in April 2006 and carry a 94-GHz cloud profiling radar (CPR) and a dual-wavelength lidar in order to provide more accurate information about cloud vertical structure. This study uses the merged product (i.e. CloudSat CPR + CALIPSO lidar cloud mask, referred to as the C–C data) to obtain low cloud fractions and to calculate de-correlation length values, as well as to illustrate global cloud overlap. This merged product provides more reliable cloud information pertaining to multi-layered clouds, such as optically thin high clouds over low-level thick clouds (Mace et al. 2009).

2.5 ARM ground-based measurements

The ARM program's ground-based products are employed to assess the existence of systematic errors in temperature, relative humidity and cloud mixing ratio fields used in the GFS model's cloud scheme. The SGP site in north-central Oklahoma is the first field measurement site established by the Department of Energy's ARM program. The site is well-equipped with a large set of instruments useful for weather and climate research and collects observations of meteorological variables that are used to test various models from detailed process models to highly parameterized models (Stokes and Schwartz 1994). Data from the site are widely employed to improve the prediction accuracy of weather forecast models and parameterization schemes (Lazarus et al. 1999; Xi et al. 2010; Sengupta et al. 2004) and to estimate cloud optical and macrophysical properties at different vertical levels (Wang and Sassen 2004; Dupont et al. 2011). High temporal resolution (about every 8 min) atmospheric emitted radiance interferometer (AERI) observations of temperature and water vapor profiles are used in this study. The ARM value-added product (VAP) of cloud condensed water observations are employed which represents the best estimates derived from several instruments. This product contains retrievals of cloud microphysical properties, such as liquid/ice water content and particle effective radius, using a combination of observations from the 35-GHz millimeter-wavelength cloud radar, the microwave radiometer, and radiosonde soundings.

3 Diagnosis of GFS model parameters

The GFS model is the operational medium-range global forecast model run by the NCEP. It uses a T382 spectral triangular truncation with a horizontal resolution of 35 km and 64 vertical layers. This study uses forecast data generated every 3 h from 00Z to 24Z for each day in July 2007 and July 2008. Forecast output fields used in this study have 21 vertical layers: from the near surface (1,000 mb) to 900 mb, the vertical resolution is 25 mb; above 900 mb, there are 16 levels at a 50 mb resolution up to 100 mb. The cloud fraction (C) in a given model grid box is diagnosed based on a prognostic condensate scheme using a combination of model-predicted three-dimensional temperature, relative humidity and cloud water mixing ratio fields (Xu and Randall 1996). More in-depth details about the GFS cloud scheme are given in Moorthi et al. (2001). Cloud fraction is calculated as follows:

$$\mathrm{C} = \max\left[R^{0.25}\left(1 - \exp\left\{-\frac{2000 \times (q_c - q_{c\min})}{\min[\max([(1-\mathrm{R}) \times \mathrm{q}^*]^{0.25}, 0.0001),\ 1.0]}\right\}\right),\ 0.0\right], \quad (1)$$

where q^* is the saturation specific humidity, R is the relative humidity, q_c is the cloud water mixing ratio, and q_{cmin} is a minimum threshold value of q_c. Clouds in the GFS model are classified according to cloud-top pressure, p: high clouds ($p < 350$ mb), mid clouds (350 mb $< p <$ 642 mb), and low clouds ($p > 642$ mb).

3.1 Evaluation of global low clouds and the radiation budget at the TOA

Figure 1 shows global distributions of low-level cloud fractions estimated from the CL algorithm applied to MODIS data and GFS model simulations. Simulated low clouds agree with satellite retrievals in terms of location. While satellite retrievals show extensive marine stratocumulus clouds over the eastern tropical Pacific and Atlantic oceans, such clouds are not well-simulated by the GFS model.

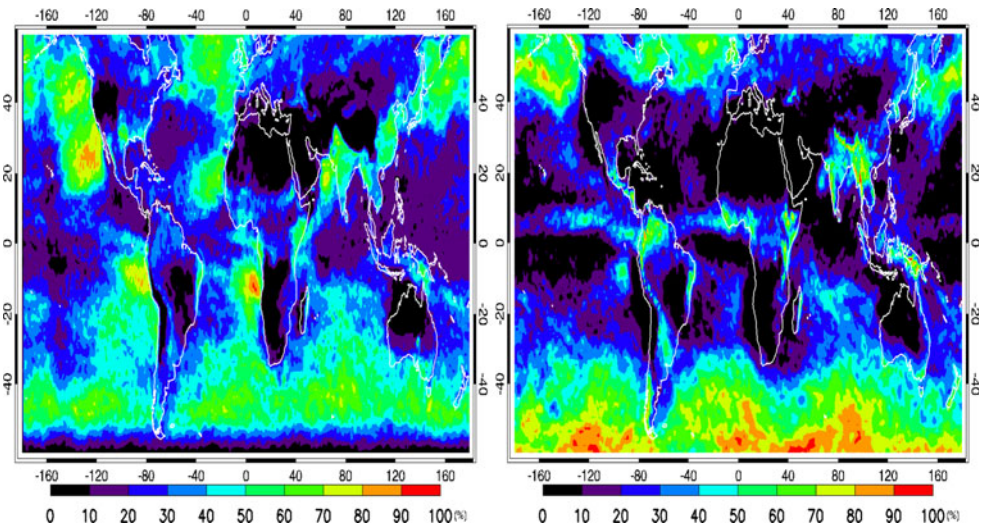

Fig. 1 Low cloud fractions from the CL algorithm (*left*) and the GFS model (*right*) in July 2008

A comparison of global distributions of monthly mean outgoing shortwave (SW), longwave (LW), and net radiation at the TOA from CERES measurements and GFS simulations is shown in Fig. 2. Net radiation at the TOA is defined as the balance between solar radiation and terrestrial radiation. Gross patterns for outgoing SW and LW radiation at the TOA are similar for both observations and simulations on a global scale, but disagreements exist over the eastern Pacific and Atlantic regions. The GFS model produces less outgoing SW radiation and more outgoing LW radiation than that measured by CERES; these radiation discrepancies are co-located with regions where stratocumulus cloud cover is underestimated. Similar results concerning radiation discrepancies were reported by Hinkelman et al. (1999) who compared output from the NCEP Eta forecast model with ground-based measurements from the SGP site and in a study using the Canadian regional climate model (Paquin-Ricard et al. 2010). Table 1 summarizes global monthly mean outgoing SW, LW, and net radiation at the TOA under all-sky conditions from CERES measurements and GFS model simulations for July 2008. Mean values of SW, LW, and net radiation for CERES (GFS) are 90.91 W/m^2 (81.13 W/m^2), 247.62 W/m^2 (252.53 W/m^2), and −2.21 W/m^2 (13.35 W/m^2), respectively. CERES-measured and model-simulated net radiation at the TOA has opposite signs, emphasizing the impact of marine stratocumulus clouds on global net radiation.

3.2 Regional analysis of cloud fraction, temperature, and relative humidity (RH)

To investigate the potential causes for the discrepancies in marine stratocumulus cloud decks between model simulations and observations, four areas along the west coasts of the America and Africa were selected and are shown in Fig. 3. Stratocumulus clouds form in these regions with cold sea surface temperature and a strong temperature inversion that caps the boundary layer. The geographic boundaries of each region are a bit arbitrary and different from those analyzed by Klein and Hartmann (1993). The individual regions here are defined as: Californian (10°–40°N, 160°–110°W), Peruvian (0°–30°S, 110°–75°W), Namibian (0°–30°S, 30°W–10°E), and Canarian (10°–40°N, 60°–20°W). Regional mean radiation fields for July 2008 are summarized in Table 2. Simulated SW fluxes at the TOA are all less than those observed from space with differences ranging from 10.67 to 24.77 W/m^2 while LW fluxes simulated by the GFS model are all greater than observed values, with differences ranging from 3.92 to 9.82 W/m^2.

Figure 4 presents a comparison of zonal mean low cloud fractions derived from both satellite retrievals and the GFS model over each region. Note that the two satellite results are generated from the application of different algorithms to the same MODIS data. The low cloud fraction derived from the CL algorithm is much greater than that retrieved by the MODIS algorithm in all regions as a result of the recovery of a large quantity of low clouds beneath high clouds. This comparison illustrates how the same satellite data might result in considerable discrepancies in low-level cloud detection depending on which algorithm was used in cloud retrievals. Retrievals based on the C–C data lie somewhere in between two MODIS results and are more similar to those from the CL algorithm. The low cloud fraction simulated by the GFS model is substantially smaller than that retrieved from satellites over all regions. These results are consistent with a previous study, which reported that the Xu and Randall cloud parameterization scheme underestimated cloud fractions when compared to observations from the Atlantic Stratocumulus Transition Experiment (Lazarus et al. 1999).

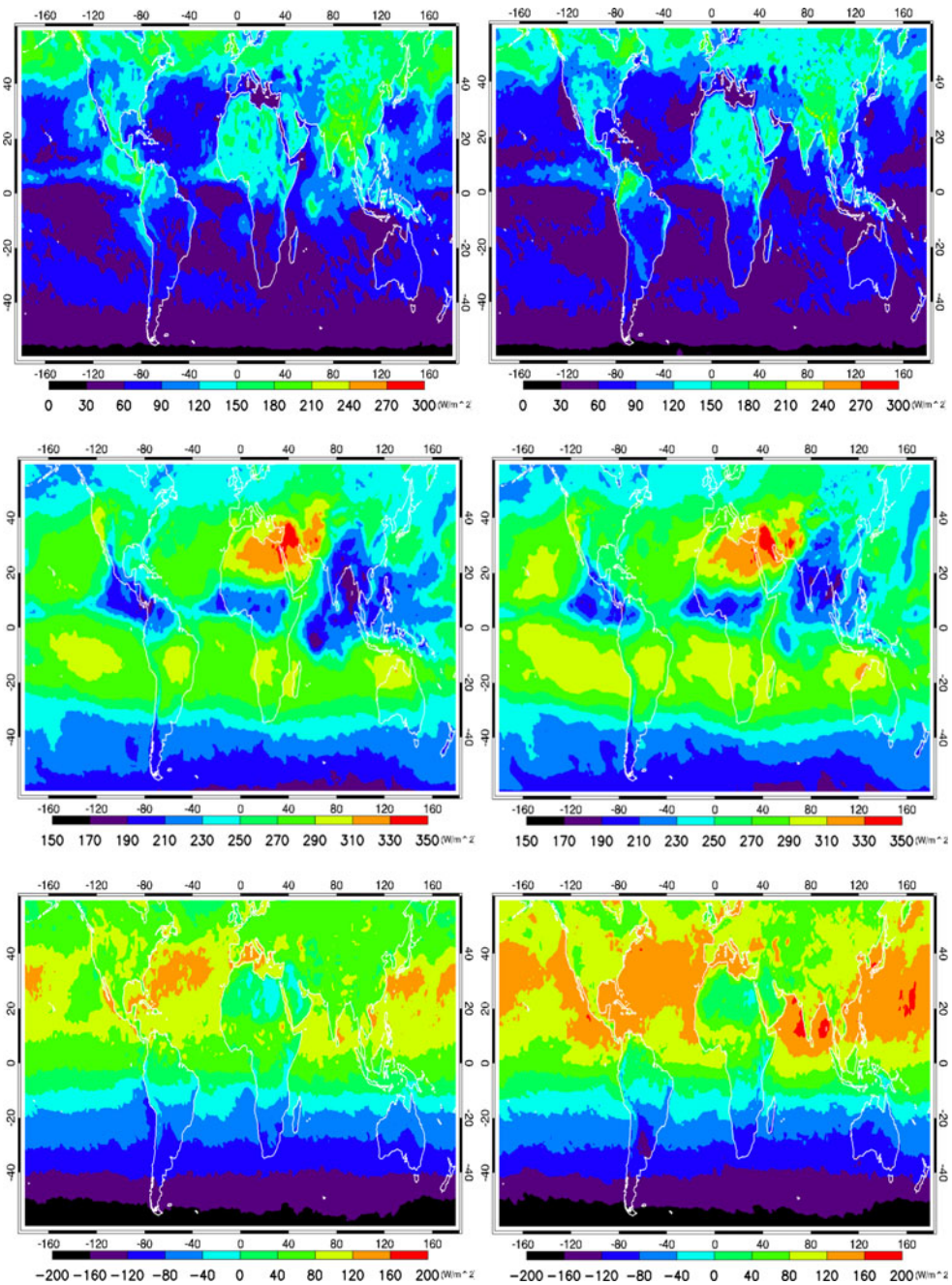

Fig. 2 Global distributions of the outgoing shortwave flux (*top*), longwave flux (*middle*), and net flux (*bottom*) at the TOA from CERES measurements (*left*) and the GFS model (*right*) in July 2008

Table 1 Global monthly mean SW, LW, and net fluxes at the TOA obtained from CERES measurements and the GFS model during July 2008

	CERES (W/m^2)	GFS (W/m^2)
SW Flux	90.91	81.13
LW Flux	247.62	252.53
Net Flux	−2.21	13.35

This study aims to analyze whether the discrepancies seen in low cloud fields arise from incorrect input variables and/or from the cloud parameterization scheme used in the GFS model. First, the input variables used in the cloud parameterization scheme are evaluated by comparing them to satellite retrievals and ground-based measurements. Figure 5 compares the zonally averaged temperature from AIRS observations and the GFS model. The agreement is only poor between 30° and 40° in the Californian cross-section but along the rest of the cross-section, the agreement is acceptable, illustrating that the model does a reasonable job of predicting zonally-averaged temperature at different altitudes. Figure 6 shows latitudinal variations of zonal-mean RH corresponding to the same four vertical levels in the atmosphere. Much less agreement is seen between

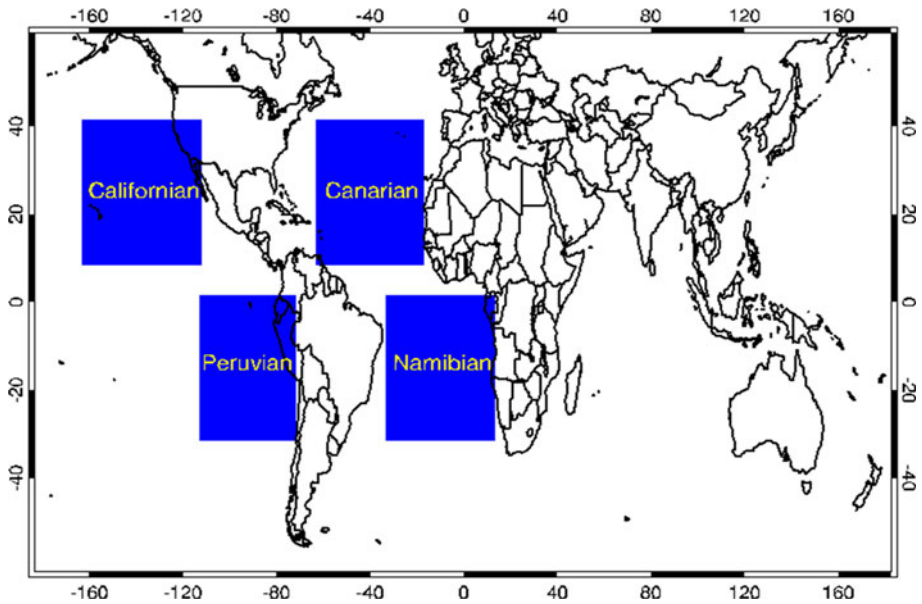

Fig. 3 Locations of the four regions under study where marine stratocumulus clouds are prevalent: Californian (10°–40°N, 160°–110°W), Peruvian (0°–30°S, 110°–75°W), Namibian (0°–30°S, 30°W–10°E), and Canarian (10°–40°N, 60°–20°W)

Table 2 Regional mean SW and LW fluxes under all-sky conditions at the TOA from CERES measurements and the GFS model over selected regions during July 2008

	CERES		GFS	
	SW (W/m^2)	LW (W/m^2)	SW (W/m^2)	LW (W/m^2)
Californian	99.15	273.22	74.38	280.04
Peruvian	79.08	274.99	56.94	284.81
Namibian	62.02	278.46	51.07	286.04
Canarian	74.46	272.47	63.79	276.39

observations and simulations. The GFS model overestimates RH values (especially at 850 mb) with differences up to double the satellite estimates in the four regions. This suggests that GFS-simulated RH values have larger systematic biases in cloud layers than do GFS-simulated temperatures, especially in marine stratocumulus cloud decks.

3.3 Comparison of temperature, RH, and cloud mixing ratio profiles with ground-based measurements

Satellite measurements provide useful atmospheric information on a global scale, but they have shortcomings such as retrieval uncertainties. Therefore, a comparison with ground-based measurements is also needed. Since there are temporal and spatial differences between satellite measurements and surface-based observations, a careful match is required. A 1° × 1° grid box centered on the SGP site is considered and AERI profiles taken 30 min before and after the Aqua overpass time were selected. Profiles that passed the data quality check were then averaged to obtain a mean profile at the overpass time and it was finally matched to AIRS retrievals. Figure 7a, b show comparisons of RH and temperature profiles from satellite retrievals, ground-based measurements, and model simulations at the SGP site during July 2008. RMS errors between AIRS (GFS-simulated) and AERI retrievals of RH and temperature are 4.06 % (15.59 %) and 6.26 K (5.91 K), respectively. Estimates of temperature from AIRS retrievals and model simulations are very similar. The agreement between the two observation-based estimates of RH is better than that between AERI-retrieved RH and GFS-simulated RH. In general, the GFS model overestimates RH in both the upper and lower troposphere.

Figure 8a shows the profiles of cloud fraction from five products: a product generated by the GFS with original model inputs, a product with the AERI retrievals of temperature and RH and cloud mixing ratio from the GFS, a product with the GFS simulations of temperature and RH and cloud mixing ratio from the VAP, a product with the AERI retrievals of temperature and RH and cloud mixing ratio from the VAP, and combined millimeter wavelength cloud radar (MMCR)-micropulse lidar (MPL) observations. The MMCR generates continuous cloud profiles from radar reflectivity and the MPL is sensitive to optically thin clouds, so combining the two types of measurements leads to more accurate estimation of cloud fraction (Xi et al. 2010). The GFS model largely underestimates low cloud fraction relative to MMCR-MPL, which is consistent with a previous study (Yang et al. 2006). Cloud fractions generated by the original GFS model (black line) are greater than those generated using temperature and RH from AERI and cloud mixing ratio from the GFS model (red line). This is due to the model's overestimation of RH. The other three cloud fraction profiles (green, blue and

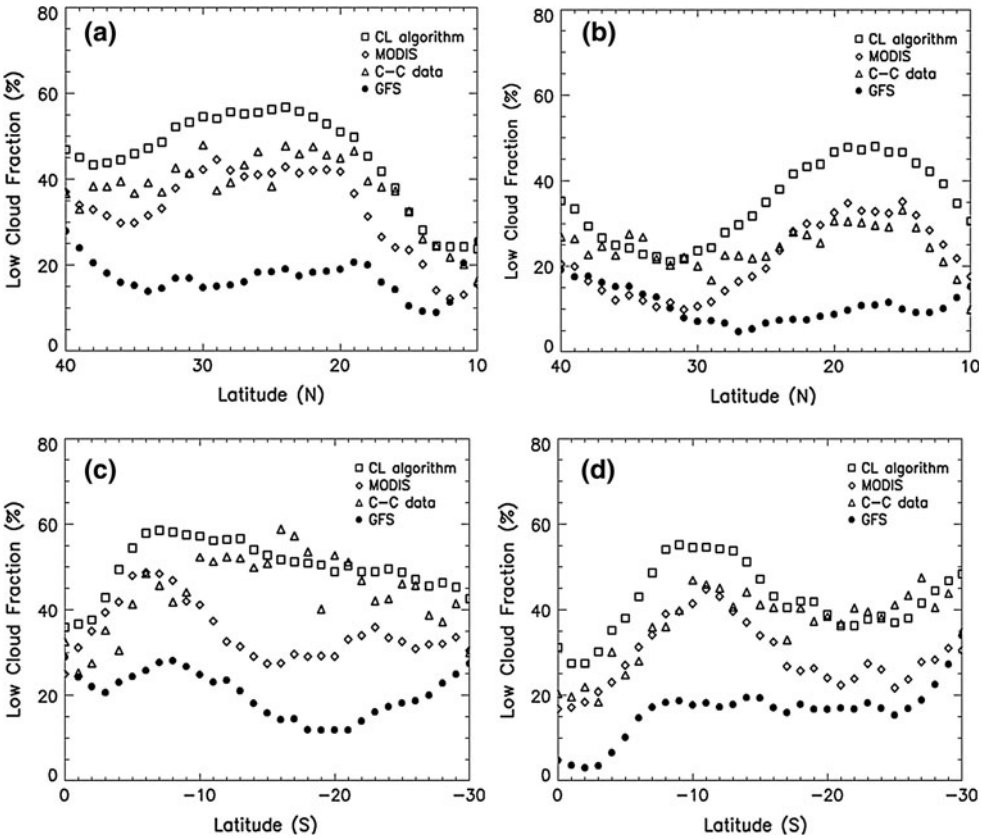

Fig. 4 Comparisons of zonal-mean low cloud fractions derived from three satellite products (MODIS-EOS, MODIS-CL, CloudSat/CALIPSO) and the GFS model for Californian (**a**), Canarian (**b**), Peruvian (**c**) and Namibian (**d**) regions in July 2008

yellow lines) agree reasonably well in the middle-to-lower troposphere. MMCR-MPL-retrieved cloud fractions (yellow line) are smaller than cloud fractions generated from using model temperature and RH and VAP-derived cloud mixing ratio (green line). As a result, use of cloud mixing ratio retrieved from the VAP, rather than replacing temperature and RH values, results in better cloud fraction estimates. It may thus be concluded that the underestimation of cloud mixing ratio in the GFS model is a primary contributor towards the error in GFS cloud fraction estimates. This statement can be reinforced from Fig. 8b. Figure 8b compares cloud condensed mixing ratios simulated by the GFS with those retrieved from the VAP at the SGP site and it shows that cloud water mixing ratios from the GFS are much smaller than those from observations in the lower troposphere, which is likely a major source of error in the modeled cloud fraction.

The underestimation of cloud water mixing ratio in the GFS model has been recognized due to the uses of an unrealistic turbulent diffusion in the shallow convective scheme and a planetary boundary layer scheme which is optimized for dry boundary layers (Han and Pan 2011). The shallow convective scheme removes cloud condensate water through strong vertical diffusion in cloud layers. As a result, simulated cloud fractions are severely underestimated over the selected regions although RH values simulated by the GFS model are mostly larger than satellite-retrieved RH values. The combined effect results in a systematic underestimation of low clouds (Han and Pan 2011). Among all GFS model input variable, the cloud water mixing ratio appears to be a primary contributor to the discrepancies found in cloud fields. GFS modelers have tried to improve the vertical mixing in the shallow convective scheme and they did update the version of the model in 2010. In order to fix the underestimation of cloud water mixing ratio, the shallow convective scheme in the latest version of the GFS model uses a mass flux parameterization which replaces the old turbulent diffusion-based approach. We compared low cloud fractions from the updated GFS model with those derived from the CL algorithm. More marine stratocumulus clouds are generated in the new version of the model but those are still underestimated.

4 Testing of an alternative cloud parameterization scheme

As an attempt to circumvent the problem associated with cloud water mixing ratio simulated by the GFS model, we tested another approach that does not use cloud water mixing ratio. Two types of schemes have typically been

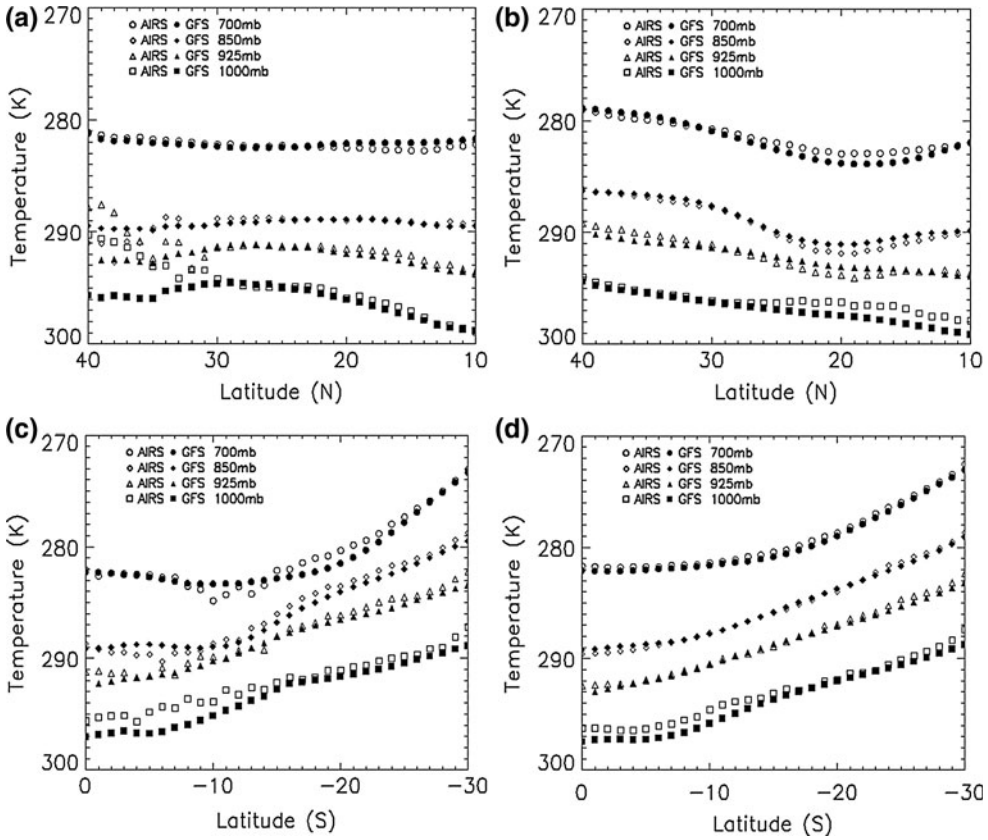

Fig. 5 Comparisons of zonal-mean temperature profiles derived from AIRS observations and the GFS model for Californian (**a**), Canarian (**b**), Peruvian (**c**) and Namibian (**d**) regions in July 2008 at 700, 850, 925, and 1,000 mb

used to determine cloudiness in models: diagnostic and prognostic schemes. In a diagnostic scheme, cloud properties are determined diagnostically and given their simplicity, these schemes have been widely used in large-scale models. In the prognostic scheme of Tiedtke (1993), the cloud fraction and cloud condensate are directly modelled. Various prognostic cloud schemes have been proposed in lieu of diagnostic cloud schemes in order to improve climatological distributions of cloud fraction, precipitation, and moisture fields such as those used in the Met Office Unified Model (Wilson et al. 2008), ECHAM5 model developed by the Max Planck Institute for Meteorology (Tompkins 2002), and Model for Interdisciplinary Research on Climate (Watanabe et al. 2009). Very sophisticated schemes were also developed for coping with boundary-layer clouds (Golaz et al. 2002; Neggers 2009). Currently, the GFS model lies somewhere in between the two types of schemes in that cloud condensed water is a prognostic variable but cloud fraction is determined diagnostically.

To avoid the use of cloud water mixing ratio as a predictor for cloud fraction, an alternative diagnostic parameterization is tested for computing cloud fraction based on Gordon (1992) as used in a previous version of the Geophysical Fluid Dynamics Laboratory model. It originated from the Slingo (1987) scheme used in a previous version of the European Center for Medium-range Weather Forecasts (ECMWF) model with modifications to the power law relationship between relative humidity and threshold relative humidity and to the parameterization of marine stratocumulus clouds. This hybrid Slingo-Gordon scheme is denoted as the SG scheme hereafter. The SG scheme computes cloudiness by an empirical formulation which accounts for convective activity and thermodynamic variables. The SG scheme was applied to the GFS model to see if it could overcome the shortcomings of the original cloud parameterization scheme used in the GFS model.

In the SG scheme, low clouds are broken down into three synoptic sub-classes: (1) low stratiform clouds (sl), (2) marine stratocumulus clouds (mcl) and (3) shallow convective clouds (shl). The cloud fraction for sub-class (1) is expressed as a product of two linear functions:

$$C_{sl} = A(RH_e) * B(\omega), \quad (2)$$

where functions A and B depend on the ambient relative humidity (RH_e) and pressure vertical velocity (ω), respectively.

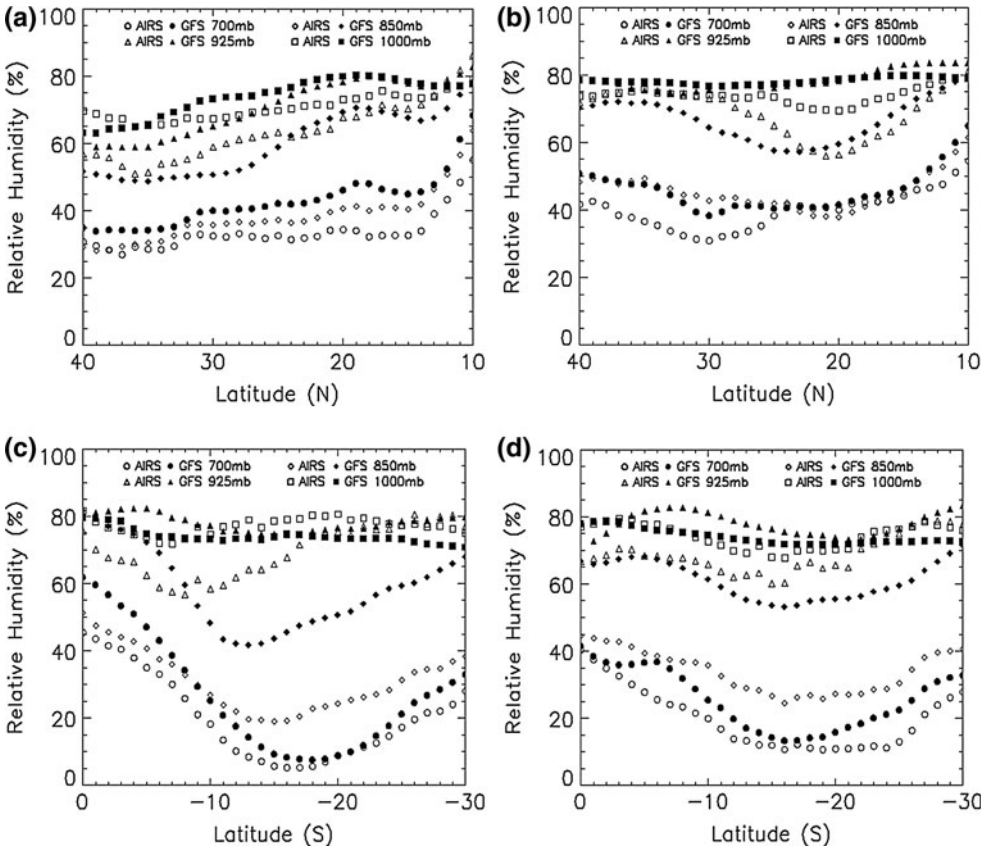

Fig. 6 Same as Fig. 5 except for relative humidity profiles

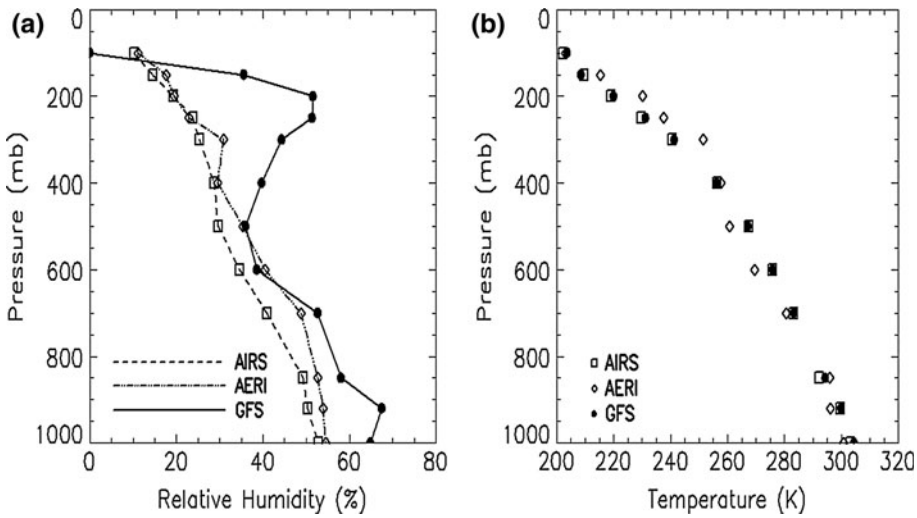

Fig. 7 Comparisons of relative humidity (*left*) and temperature (*right*) values in July 2008 from AIRS, AERI, and GFS

$$\mathrm{A}(RH_e) = \begin{bmatrix} 0.0 \\ (RH_e - RH_c)^2/(1.0 - RH_c)^2 \\ 1.0 \end{bmatrix}, \quad \text{if} \begin{bmatrix} RH_e < RH_c \\ RH_c \le RH_e \le 1.0 \\ RH_e > 1.0 \end{bmatrix}, \tag{3}$$

where RH_e is defined as RH $\times$ (1.0 $-$ C_{cnv}) and C_{cnv} is the convective cloud fraction provided by the GFS model (Pan and Wu 1995). The default coefficients for RH_c are 0.80 and 0.84 for $p < 750$ and $p \ge 750$ mb, respectively, where p is the pressure. The other linear function is expressed as

$$\mathrm{B}(\omega) = \begin{bmatrix} 1 \\ (\omega - \omega_1)/(\omega_0 - \omega_1) \\ 0 \end{bmatrix}, \quad \text{if} \begin{bmatrix} \omega < \omega_0 \\ (\omega_0 \le \omega \le \omega_1) \\ \omega > \omega_1 \end{bmatrix}, \tag{4}$$

where $\omega_0 = 0$ and $\omega_1 = 3.6$ hPa/h (Slingo 1987). Cloud fractions are greater when there is vertical ascent as opposed to descent for the sub-class (1).

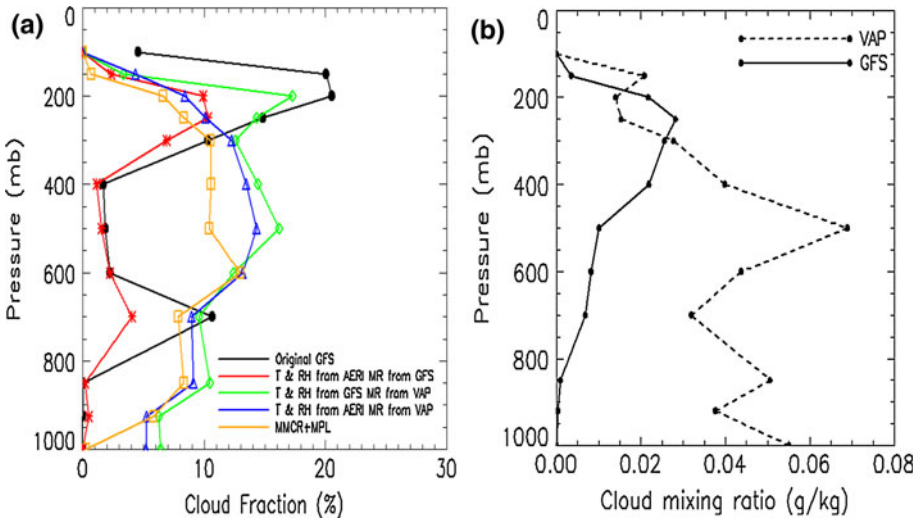

Fig. 8 Comparisons between observation and GFS model at the SGP site in July 2008 for **a** cloud fractions from five different products—the GFS original output (*black*), a product using AERI temperature and RH measurements and cloud mixing ratio from the GFS (*red*), a product using GFS-simulated temperature and RH and cloud mixing ratio from VAP (*green*), a product using AERI temperature and RH measurements and cloud mixing ratio from VAP (*blue*) and the combined radar-lidar observation product (*yellow*); **b** cloud water mixing ratio from ARM/VAP and the GFS model

The parameterization of marine stratocumulus clouds in the SG scheme resembles the formulation of Gordon (1992) and Slingo (1987). Note that RH in Eq. (5) is the relative humidity at the base of the inversion layer and an inversion layer is defined based on the sign of ∂θ/∂p, where θ is the potential temperature. The existence of a low-level inversion is not considered in the GFS model, but in other studies (e.g. Sun et al. 2010), consideration of a low-level inversion enhances the generation of stratocumulus clouds in the southeast Pacific region. In a manner similar to low stratiform clouds, the parameterization of marine stratocumulus cloud fraction is a product of two functions:

$$C_{mcl} = S\left(-\frac{\partial\theta}{\partial p}\right) * B(RH), \tag{5}$$

where θ is the potential temperature and ∂θ/∂p is the lapse rate (K/hPa). The first term on the right-hand side of the equation is defined as

$$S\left(-\frac{\partial\theta}{\partial p}\right) = \begin{bmatrix} 1.0 \\ \alpha\left(-\frac{\partial\theta}{\partial p}\right) + \beta \\ 0.0 \end{bmatrix}, \quad \text{if} \begin{bmatrix} \left(-\frac{\partial\theta}{\partial p}\right) > 0.10 \\ 0.05 \le \left(-\frac{\partial\theta}{\partial p}\right) \le 0.10 \\ \left(-\frac{\partial\theta}{\partial p}\right) < 0.05 \end{bmatrix}, \tag{6}$$

where α is 20 hPa/K and β is −1.0. The stratification criteria for marine stratocumulus clouds in the SG scheme is less stringent than that in the study of Gordon (1992), where α is 6.67 hPa/K and β is −0.667. The second term on the right-hand side of Eq. (5) is expressed as

$$B(RH) = \begin{bmatrix} 1 \\ (RH - RH_{\min})/(RH_{\max} - RH_{\min}) \\ 0 \end{bmatrix}, \quad \text{if} \begin{bmatrix} RH > RH_{\max} \\ RH_{\min} \le RH \le RH_{\max} \\ RH < RH_{\min} \end{bmatrix}, \tag{7}$$

where the default values for RH_{min} and RH_{max} are 0.60 and 0.80, respectively (Gordon 1992).

The shallow convective cloud fraction is calculated as

$$C_{shl} = 0.2 \times A(RH_{e,\max}) \tag{8}$$

The function A is from Eq. (3) and $A(RH_{e,\max})$ is the maximum value of RH_e for $p \ge 750$ mb.

In summary, the low cloud fraction is obtained by applying the maximum overlap assumption:

$$C_{low} = \text{Max}[C_{sl}, C_{mcl}, C_{shl}]$$

Figure 9 shows the comparison between the cloud fraction generated from observations using the CL algorithm and the model product generated from the application of the SG scheme to the GFS model. Using the GFS model with the SG scheme rather than the original GFS cloud output resulted in an increase in mean low cloud fraction during July 2008 from 31.6 to 40.8 %. This is comparable with the observed cloud fraction of 38.6 %. More marine stratocumulus clouds are now generated in all four regions and latitudinal variations in zonal-mean low cloud fractions agree well with the patterns seen in satellite

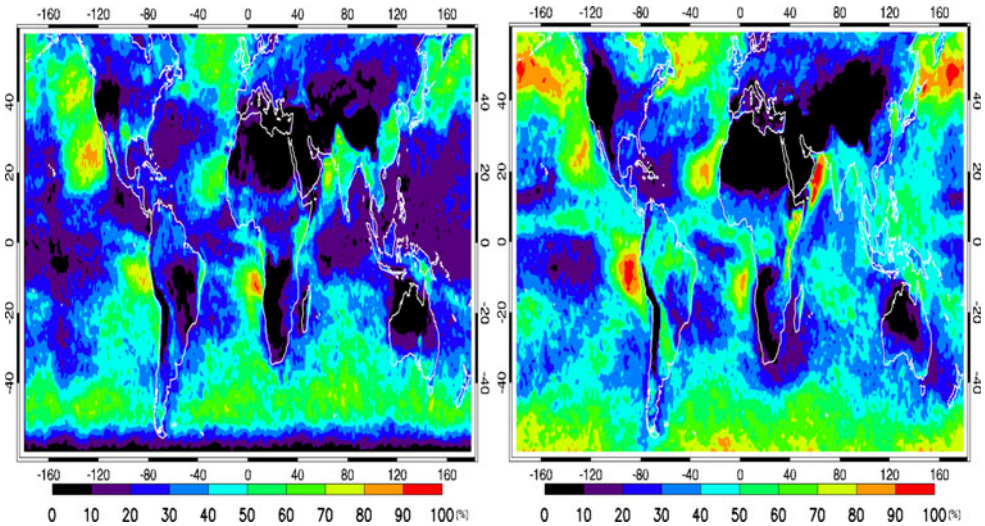

Fig. 9 Low cloud fractions from the CL algorithm (*left*) and from the GFS model using the SG scheme (*right*) in July 2008

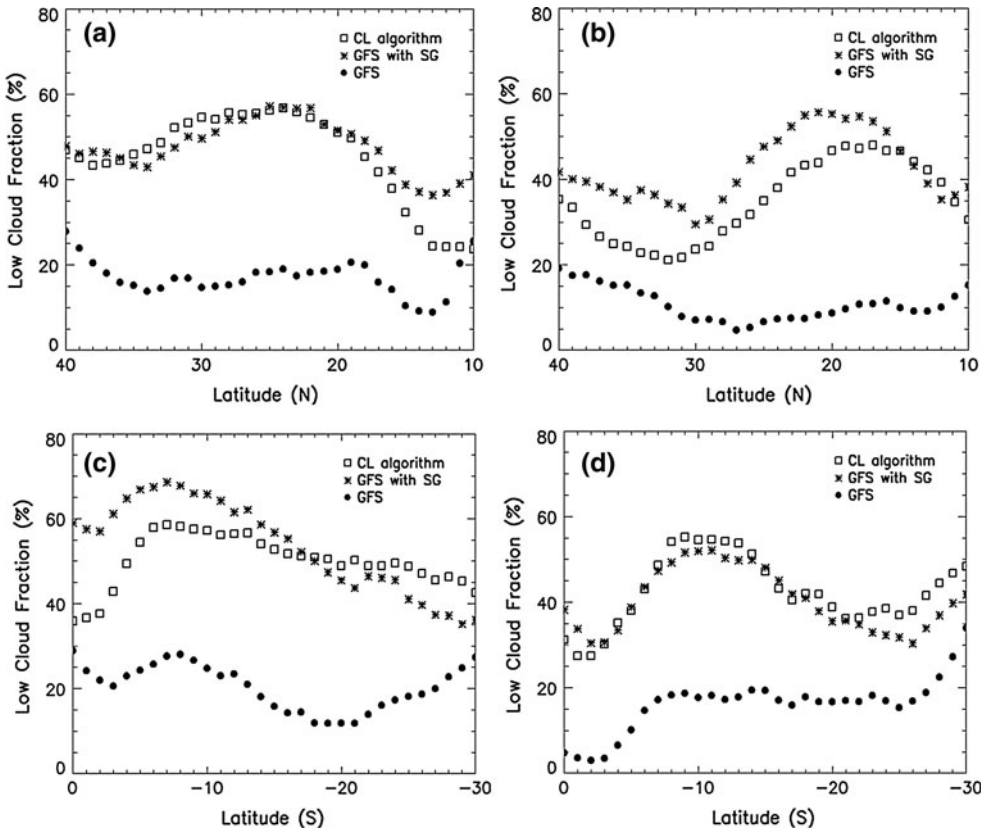

Fig. 10 Latitudinal variations of zonal-mean low cloud fractions over the four regions from the CL algorithm, the GFS model using the SG scheme, and the GFS model in its original form

observations (see Fig. 10). In particular, very good agreement is seen in the Californian and Namibian regions.

5 Impact of the cloud overlap assumption

For a given profile of layer-by-layer cloud fractions in a model, the total cloud fraction may differ substantially depending on the cloud overlap assumption used (Morcrette and Jakob 2000; Collins 2001). GCMs generally parameterize cloud fraction in a given model grid box since the horizontal resolution of GCMs is much coarser than the scale of clouds. The discrepancies in radiative fluxes shown in Sect. 3.1 may originate from discrepancies in column cloud fraction that are determined from cloud fractions at individual model levels and the assumption of cloud overlap, which is significant to climate modeling (Liang and Wu 2005). The global verification of cloud

overlap assumptions is now feasible given observations of cloud vertical structure obtained from passive (Chang and Li 2005b) and active (Barker 2008; Mace et al. 2009) satellite sensors. These observations can be augmented through the use of ground-based data from active remote sensing (Oreopoulos and Norris 2011).

There are three basic cloud overlap assumptions: maximum, random, maximum-random, and minimum overlap (Hogan and Illingworth 2000). Maximum overlap assumes that cloud layers are overlapped as much as possible; minimum overlap assumes the opposite. Random overlap assumes that the horizontal positions of clouds in any pair of layers are completely uncorrelated. Morcrette and Jakob (2000) showed how different total cloud fraction could be for mid-latitude summer atmosphere, depending on the choice of overlap assumption: 30 % if the maximum overlap assumption was used and 65.7 % if the random assumption was used. Choice of overlap assumption could also result in errors in instantaneous solar flux estimates on the order of several hundred W/m^2 (Barker et al. 1999).

The maximum-random overlap (MRO) assumes that clouds in contiguous layers are maximally overlapped while clouds in non-contiguous layers are randomly overlapped (Geleyn and Hollingsworth 1979). Some operational models use the MRO assumption (Barker 2008). A study by Tian and Curry (1989) quantitatively evaluated the MRO method using the 15-level US Air Force 3-D Nephanalysis over the north Atlantic Ocean and showed that the MRO assumption describes characteristics of cloud vertical structure fairly well.

The MRO assumption, however, fails to capture all the details of cloud overlap in the real atmosphere. Hogan and Illingworth (2000) evaluated the MRO assumption using millimeter-wave cloud radar profiles for three winter months at Chilbolton in the United Kingdom and found that the degree of correlation between cloud layers is determined by the vertical distance between any two cloud layers. They suggested that the MRO assumption could be modified to include a weighting factor that depends on a de-correlation length and the separation distance. In this modified MRO assumption, cloud overlap lies somewhere between maximum and random and it is referred to as exponential random overlap (ERO). The vertically-projected total cloud fraction (C_{ERO}) is then determined by the linear combination of maximum and random overlap as

$$C_{ERO} = \alpha C_{max} + (1 - \alpha) C_{ran} \tag{9}$$

where

$$\begin{aligned} C_{max} &= \mathrm{Max}(C1, C2), \\ C_{ran} &= C1 + C2 - C1 \times C2, \end{aligned} \tag{10}$$

and C1 and C2 are the respective cloud fractions of the two cloud layers. The value of the weighting factor, alpha, is defined as

$$\alpha = \exp\left(\frac{-\Delta z}{Lcf}\right) \tag{11}$$

where L_{cf} is the de-correlation length and Δz is the vertical distance between the two layers of cloud. The value of α ranges from 0 for pure random overlap to 1 for maximum overlap. The value of L_{cf} is ultimately determined by cloud regimes but here, it is related to the vertical resolution and horizontal domain size. A number of studies, using millimeter radar data from either ground-based or satellite-based instruments, or output from cloud-resolving models, have suggested different values for α (Mace and Benson-Troth 2002; Oreopoulos and Khairoutdinov 2003; Pincus et al. 2005; Naud et al. 2008). Barker (2008) performed a global study of cloud overlap properties using the C–C data and found a wide range of L_{cf} with a median value of 2 km. Shonk et al. (2010) proposed a simple linear relationship between L_{cf} and latitude based on two previous studies.

To minimize the discrepancies caused by the choice of overlap assumptions when we come to compare the model cloud fraction to the observations, we follow Barker (2008) to determine L_{cf} from the C–C data for use with the GFS. Note that one satellite orbit contains 37,081 profiles, each approximately 1.4 km wide and 1.1 km along-track, with a vertical grid-spacing of 0.24 km. The lowest 1 to 3 bins next to the surface are not considered because they are contaminated by ground clutter. CPR cloud mask and radar reflectivity variables from the 2B-GEOPROF product and the cloud fraction field from the 2B-GEOPROF-LIDAR product are utilized. For this study, values <20 in the CPR cloud mask field are selected to reduce the probability of a false detection of cloud (Stephens et al. 2002). The data screening for cloud detection consists of a sequence of tests for three conditions (Barker 2008):

$$\begin{aligned} &CPR\_cloud\_mask \geq 20 \\ &radar\_reflectivity \geq -30\,dBZ \\ &\text{Or} \\ &CPR\_cloud\_mask < 20 \\ &cloud\_fraction \geq 99\,\% \\ &radar\_reflectivity \geq -30\,dBZ \end{aligned} \tag{12}$$

A stochastic sub-grid-scale cloudy column generator developed by Räisänen et al. (2004) is then used to produce synthetic sub-grid-scale columns of cloud for comparing against cloud fraction derived from observations. Fifty thousand sub-columns are generated for each cross-section of 500 km length. The effective L_{cf} that satisfies the observed cloud fraction is found using Brent's root-finding technique (Brent 1973). The range of admissible solutions for L_{cf} is bounded between 0.05 and 20 km.

Figure 11 illustrates the spatial variation of median values of L_{cf} for high, mid, low clouds and their variations as a function of total cloud fraction for July 2007. Overall, there is considerable variability in L_{cf} due to the influence of extreme values of L_{cf}. Median values of L_{cf} for mid clouds are large because mid clouds are usually well-organized. As per Chang and Li (2005b), global clouds have two predominant modes in terms of cloud top location: low and high with few clouds with tops in the mid atmosphere. This suggests the majority of cloud remain either in the low atmosphere as boundary layer clouds, in the high atmosphere as cirrus clouds, or penetrate through the bulk of troposphere as deep clouds. Such a dominant pattern of cloud vertical distribution explains why L_{cf} for mid-level clouds is particularly large relative to low and high clouds, as mid clouds are more strongly correlated than low and high clouds. The bottom panel of Fig. 11 shows the overall variations of L_{cf} with total cloud fraction within three representative layers: high, mid and low. Quadratic fits to the curves are

$$\begin{aligned} L_{cf\_high} &= -4.27\mathrm{C}^2 + 4.60\mathrm{C} + 0.88 \\ L_{cf\_mid} &= -9.50\mathrm{C}^2 + 10.72\mathrm{C} + 1.49 \\ L_{cf\_low} &= -5.06\mathrm{C}^2 + 6.40\mathrm{C} + 0.35 \end{aligned} \quad (13)$$

for high, mid, low clouds, respectively. As total cloud fraction changes, the median values of L_{cf} for high and low clouds show a similar pattern that differs from that for mid clouds. The relative coarseness of the vertical grid can be a problem in dealing with thermodynamic properties (Boutle and Morcrette 2010). Although we could use the Boutle and Morcrette method to sharpen the thermodynamic profile near the inversion and hence increase relative humidity there before diagnosing cloud fraction, we have not tried it and this is an area for possible future consideration.

We perform two experiments to show the relative importance of changing from cloud scheme to cloud overlap assumption. By applying the ERO with observation-based estimates of L_{cf} both to the original vertical distribution of cloud fraction from the GFS model and to cloud fraction using the SG scheme, cloud fractions are determined for three representative layers. Figure 12 compares cloud fractions for the three layers from the original GFS cloud product, a product generated from Xu and Randall scheme using the ERO overlap assumption, and cloud fraction calculated from the SG scheme using the ERO overlap assumption against cloud fractions derived from the CL algorithm using MODIS data. Overestimation of high-level cloud fractions from the original GFS model (Yoo and Li 2012) is dramatically improved when the observation-based overlap assumption with the Xu and Randall scheme is used. Mid-level cloud fractions are similar in terms of location and magnitude. The two experiments generate slightly less mid-level cloud fractions compared to the original GFS cloud product. For low-level clouds, however, the product generated from the Xu and Randall scheme using the ERO overlap assumption tends to reduce low cloud fraction, thereby worsening the agreement with satellite retrievals. The low-level cloud fraction from the SG scheme with the ERO overlap assumption is more generated than the observed cloud fraction. Based on this comparison, we can infer that poor layer cloud fractions calculated from the original GFS cloud scheme with the ERO overlap assumption cannot be expected to solve the problem. Overall, the change in cloud scheme, and not overlap assumption, has the most impact on modeling more realistic cloud fields.

6 Summary

Understanding low cloud properties and their spatiotemporal variations, a problem faced by GCMs, is crucial for studying global climate change. Taking advantage of the wealth of information regarding the global distribution of cloud properties and atmospheric variables from various satellite sensors, we examined low cloud fractions, meteorological variables, and the cloud parameterization scheme of the GFS model with reference to satellite retrievals and ground-based measurements made during July 2007 and July 2008. The GFS model generates a sound spatial pattern of low clouds but large discrepancies exist in low cloud fraction over the eastern tropical oceans. The MODIS standard product and a new MODIS-based research product generated with the algorithm of Chang and Li (2005a) show more stratocumulus clouds than those predicted by the GFS model. An underestimation of marine stratocumulus clouds leads to more outgoing longwave radiation and less shortwave radiation at the TOA over those regions. To diagnose the causes of the bias in simulated cloud fractions, both input variables and cloud parameterization schemes are examined using a large variety of observation data from a suite of satellite sensors and ground-based measurements.

The GFS temperature field agrees well with AIRS observations at different vertical levels, but relative humidity is overestimated in both the upper and lower troposphere. Consistent results are found when comparing against ground-based measurements made at the ARM SGP site. This is somewhat contradictory with the finding that GFS underestimates substantially low-level cloud fractions. The underestimation of low-level cloud fraction appears to stem from severe underestimation of cloud condensate water which is a key input variable to the parameterization scheme of Xu and Randall (1996). It appears that cloud condensate water is removed too quickly

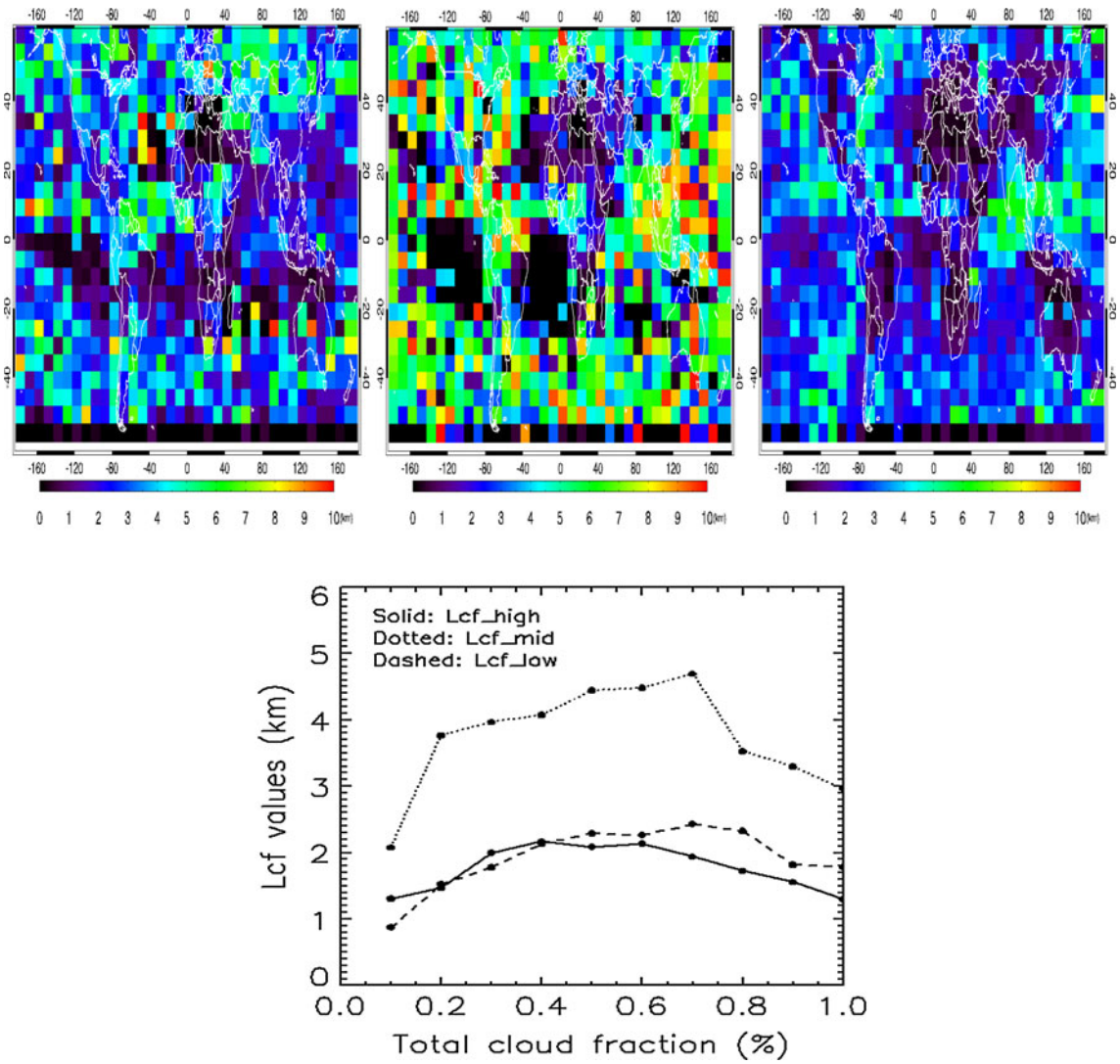

Fig. 11 *Upper panels* geographic distributions of median values of L_{cf} for high clouds (*left*), mid clouds (*middle*), low clouds (*right*) using a stochastic cloud generator and the C–C data collected in July 2007. *Lower panel* median values of L_{cf} for high, mid, low clouds as a function of total cloud fraction

by strong vertical diffusion in the shallow convective scheme used in the GFS model. Other possible causes might be related to cloud microphysics or precipitation schemes. Microphysical processes interacting with stratocumulus clouds can play a part in removing cloud condensate water quickly, as noted by Boutle and Abel (2012). Use of a prognostic cloud scheme rather than a diagnostic cloud scheme can help reduce biases in the occurrence frequencies of low, mid and high cloud fractions (Morcrette et al. 2012).

To circumvent the problem, an alternative cloud parameterization scheme that does not have the input of cloud mixing ratio is tested. We used the same thermodynamic variables from the GFS model as input to the scheme of Gordon (1992) and Slingo (1987) (denoted as SG) for computing cloud fraction. The SG scheme allows for consideration of dynamical stability and convective activity in diagnosing cloud fraction. The SG scheme leads to more marine stratocumulus clouds, as well as to more low-level clouds in other regions around the world. The spatial distribution of low clouds and zonally-averaged cloud fractions are more comparable with satellite retrievals over the regions selected for this study. The other experiment is concerned with the overlap of clouds in different layers. For a given set of cloud fractions at various model levels, cloud fraction for three representative layers depends on how clouds are arranged vertically. We applied a linear combination of maximum and random overlap scheme with a weighted factor that is a function of de-correlation length (L_{cf}) and separation distance. The spatial distribution of L_{cf} varies greatly and appears to be a quadratic curve to the total cloud fraction. Use of the

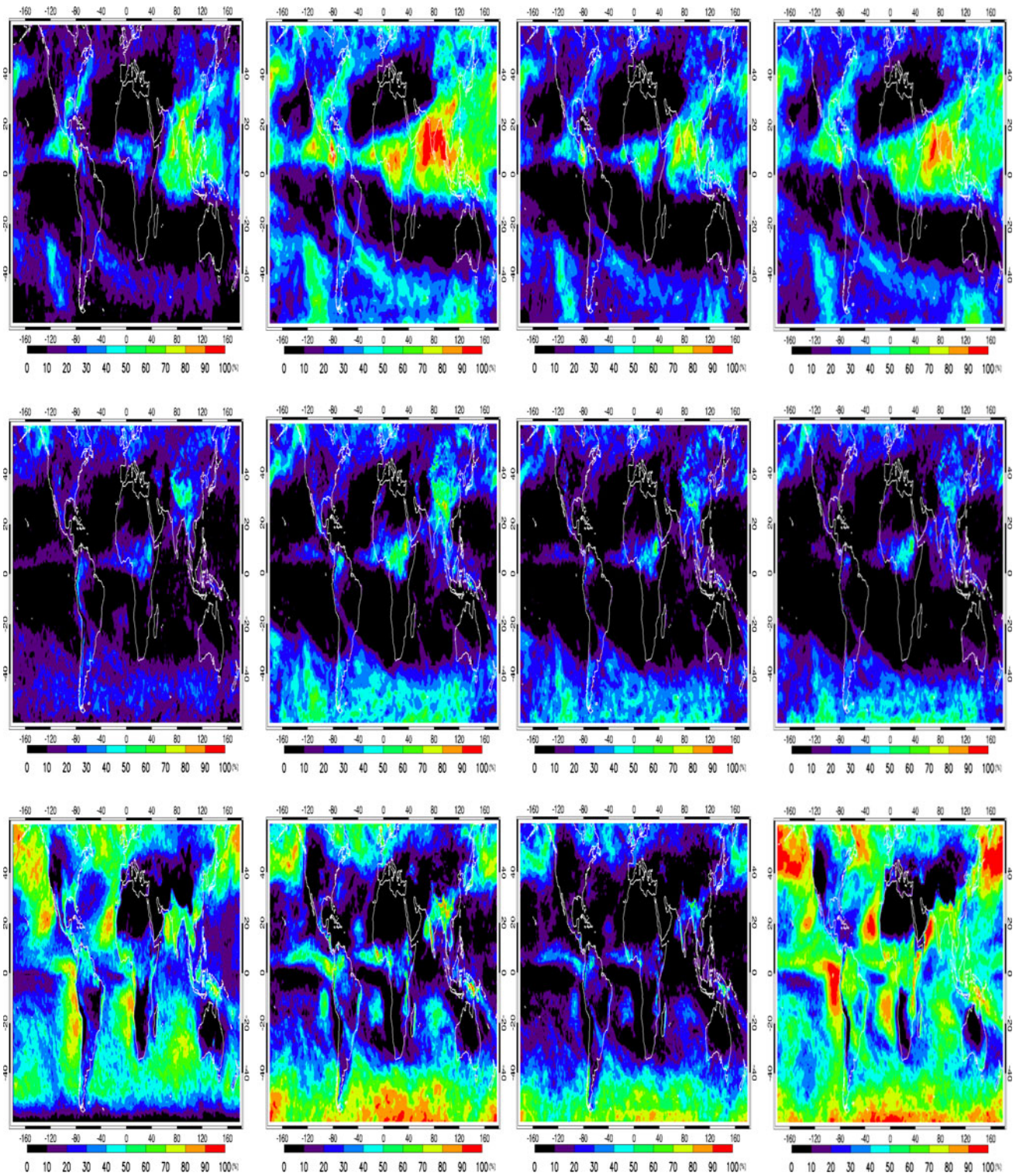

Fig. 12 Comparison of cloud fractions derived from the CL algorithm using MODIS data (*left*), the original GFS model cloud fraction (*middle left*), the original GFS cloud fraction with L_{cf} based on observations (*middle right*), and the SG scheme with L_{cf} based on observations (*right*) for high clouds (*upper*), mid clouds (*middle*), and low clouds (*bottom*) in July 2007

observation-constrained L_{cf} leads to an improvement for high-level clouds, has a neutral impact for mid-level clouds and deterioration for low-level clouds.

In summary, we conclude that discrepancies found in GFS-modeled cloud fields arise mainly from an improper treatment of the cloud water mixing ratio and that this

problem can be overcome by using the SG cloud scheme which is inherently linked with model dynamic and thermodynamic conditions and does not depend on the condensate amount. Such findings may offer guidance toward improving GFS-simulated cloud fields.

Acknowledgments We are grateful to Drs. Brad Ferrier and Shrinivas Moorthi of NOAA/NCEP for their helps with the GFS model. The authors have been supported by grants of the National Basic Research Program (2013CB955804), NSF(AGS1118325), NASA (NNX08AH71G) and DOE (DESC0007171), and NOAA GOES-R program.

References

Ackerman SA, Strabala KI, Menzel WP, Frey RA, Moeller CC, Gumley LE (1998) Discriminating clear-sky from clouds with MODIS. J Geophys Res 103:32, 141–32, 158

Ahlgrimm M, Forbes R (2012) The impact of low clouds on surface shortwave radiation in the ECMWF model. Mon Weather Rev. doi:10.1175/MWR-D-11-00316.1

Ahlgrimm M, Köhler M (2010) Evaluation of trade cumulus in the ECMWF model with observations from CALIPSO. Mon Weather Rev. doi:10.1175/2010MWR3320.1

Aumann HH et al (2003) AIRS/AMSU/HSB on the aqua mission: design, science objectives, data products, and processing systems. IEEE T Geosci Remote 41:253–264

Barker HW (2008) Overlap of fractional cloud for radiation calculations in GCMs: a global analysis using CloudSat and CALIPSO data. J Geophys Res. doi:10.1029/2007JD009677

Barker HW, Stephens GL, Fu Q (1999) The sensitivity of domain averaged solar fluxes to assumptions about cloud geometry. Q J R Meteorol Soc 125:2127–2152

Barnes WL, Pagano TS, Salomonson VV (1998) Prelaunch characteristics of the moderate resolution imaging spectroradiometer (MODIS) on EOS-AM1. IEEE T Geosci Remote 36:1088–1100

Bony S, Dufresne JL (2005) Marine boundary layer clouds at the heart of tropical cloud feedback uncertainties in climate models. Geophys Res Lett. doi:10.1029/2005GL023851

Boutle IA, Abel SJ (2012) Microphysical controls on the stratocumulus topped boundary-layer structure during VOCALS-REx. Atmos Chem Phys. doi:10.5194/acp-12-2849-2012

Boutle IA, Morcrette CJ (2010) Parametrization of area cloud fraction. Atmos Sci Lett. doi: 10.1002/asl.293

Brent RP (1973) Algorithms for minimization without derivatives. Englewood Cliffs, New Jersey

Chahine MT et al (2006) The atmospheric infrared sounder (AIRS): improving weather forecasting and providing new data on greenhouse gases. Bull Am Meteor Soc. doi:10.1175/BAMS-87-7-911

Chang FL, Li Z (2005a) A new method for detection of cirrus overlapping water clouds and determination of their optical properties. J Atmos Sci 62:3993–4009

Chang FL, Li Z (2005b) A near-global climatology of single-layer and overlapped clouds and their optical properties retrieved from Terra/MODIS data using a new algorithm. J Clim 18:4752–4771

Clothiaux EE, Ackerman TP, Mace GG, Moran KP, Marchand RT, Miller M, Martner BE (2000) Objective determination of cloud heights and radar reflectivities using a combination of active remote sensors at the ARM CART Sites. J Appl Meteor 39:645–665

Collins WD (2001) Parameterization of generalized cloud overlap for radiative calculations in general circulation models. J Atmos Sci 58:3224–3242

Dai A, Trenberth KE (2004) The diurnal cycle and its depiction in the community climate system model. J Clim 17:930–951

de Szoeke SP, Wang Y, Xie SP, Miyama T (2006) Effect of shallow cumulus convection on the eastern Pacific climate in a coupled model. Geophys Res Lett. doi:10.1029/2006GL026715

Divakarla MG, Barnet CD, Goldberg MD, McMillin LM, Maddy E, Wolf W, Zhou L, Liu X (2006) Validation of atmospheric infrared sounder temperature and water vapor retrievals with matched radiosonde measurements and forecasts. J Geophys Res. doi:10.1029/2005JD006116

Dupont JC, Haeffelin M, Morille Y, Comstock JM, Flynn C, Long CN, Sivaraman C, Newson RK (2011) Cloud properties derived from two lidars over the ARM SGP site. Geophys Res Lett doi:10.1029/2010GL046274

Geleyn JF, Hollingsworth A (1979) An economical analytical method for the computation of the interaction between scattering and line absorption of radiation. Contrib Atmos Phys 52:1–16

Golaz JC, Larson VE, Cotton WR (2002) A PDF-based model for boundary layer clouds. Part I: method and model description. J Atmos Sci 59:3540–3551

Gordon CT (1992) Comparison of 30-day integrations with and without cloud-radiation interaction. Mon Weather Rev 120:1244–1277

Han J, Pan HL (2011) Revision of convection and vertical diffusion schemes in the NCEP global forecast system. Weather Forecast 26:520–533

Hannay C et al (2009) Evaluation of forecasted southeast Pacific stratocumulus in the NCAR, GFDL, and ECMWF models. J Clim 22:2871–2889

Hartmann DL et al (1992) The effect of cloud type on Earth's energy balance: global analysis. J Clim 5:1281–1304

Hinkelman LM, Ackerman TP, Marchand RT (1999) An evaluation of NCEP Eta model predictions of surface energy budget and cloud properties by comparison with measured ARM data. J Geophys Res 104(16):19535–19594

Hogan RJ, Illingworth AJ (2000) Deriving cloud overlap statistics from radar. Q J R Meteorol Soc 128:2903–2909

Houghton JT (2001) The scientific basis. Contributions of working group i to the third assessment report of the intergovernmental panel on climate change. Cambridge University Press, Cambridge

King MD et al (2003) Cloud and aerosol properties, precipitable water, and profiles of temperature and humidity from MODIS. IEEE T Geosci Remote 41:442–458

Klein SA, Hartmann DL (1993) The seasonal cycle of low stratiform clouds. J Clim 6:1587–1606

Lazarus SM, Krueger SK, Frisch SA (1999) An evaluation of the Xu-Randall cloud fraction parameterization using ASTEX data. Preprints, 13th symposium on boundary layers and turbulence, Dallas, Texas, pp 582–585

Liang XZ, Wu X (2005) Evaluation of a GCM subgrid cloud-radiation interaction parameterization using cloud-resolving model simulations. Geophys Res Lett. doi:10.1029/2004GL022301

Loeb NG et al (2007) Multi-instrument comparison of top-of-atmosphere reflected solar radiation. J Clim 20(3):575–591

Ma CC, Mechoso CR, Robertson AW, Arakawa A (1996) Peruvian stratus clouds and the tropical Pacific circulation: a coupled ocean-atmosphere GCM study. J Clim 9:1635–1645

Mace GG, Benson-Troth S (2002) Cloud-layer overlap characteristics derived from long-term cloud radar data. J Clim 15:2505–2515

Mace GG, Zhang Q, Vaughn M, Marchand R, Stephens G, Trepte C, Winker D (2009) A description of hydrometeor layer occurrence statistics derived from the first year of merged CloudSat and CALIPSO data. J Geophys Res. doi:10.1029/2007JD009755

Mechoso CR et al (1995) The seasonal cycle over the tropical Pacific in coupled ocean-atmosphere general circulation models. Mon Weather Rev 123:2825–2838

Menzel WP, Baum BA, Strabala KI, Frey RA (2002) Cloud top properties and cloud phase algorithm theoretical basis document. http://modis.gsfc.nasa.gov/data/atbd/atbd_mod04.pdf

Moorthi S, Pan HL, Caplan P (2001) Changes to the 2001 NCEP operational MRF/AVN global analysis/forecast system. NWS Tech Proced Bull 484:14

Morcrette JJ, Fouquart Y (1986) The overlapping of cloud layers in shortwave radiation parameterizations. J Atmos Sci 43:321–328

Morcrette JJ, Jakob C (2000) The response of the ECMWF model to changes in the cloud overlap assumption. Mon Weather Rev 128:1707–1732

Morcrette CJ, O'Connor EJ, Petch JC (2012) Evaluation of two cloud parametrization schemes using ARM and Cloudnet observations. Q J R Meteorol Soc. doi:10.1002/qj.969

Naud CM, Del Genio A, Mace GG, Benson S, Clothiaux EE, Kollias P (2008) Impact of dynamics and atmospheric state on cloud vertical overlap. J Clim. doi:10.1175/2007JCLI1828.1

Neggers R (2009) A dual mass flux framework for boundary layer convection Part II: clouds. J Atmos Sci 66:1489–1506

Norris JR (1998) Low cloud type over the ocean from surface observations. Part II: geographical and seasonal variations. J Clim 11:383–403

Oreopoulos L, Khairoutdinov MF (2003) Overlap properties of clouds generated by a cloud-resolving model. J Geophys Res. doi:10.1029/2002JD003329

Oreopoulos L, Norris PM (2011) An analysis of cloud overlap at a midlatitude atmospheric observation facility. Atmos Chem Phys. doi:10.5194/acp-11-5557-2011

Pagano TS, Auman HH, Hagan DE, Overoye K (2003) Prelaunch and in-flight radiometric calibration of the atmospheric infrared sounder (AIRS). IEEE T Geosci Remote 41:265–273

Pan HL, Wu WS (1995) Implementing a mass flux convective parameterization package for the NMC medium-range forecast model. NMC Office Note 409

Paquin-Ricard D, Jones C, Vaillancourt PA (2010) Using ARM observations to evaluate cloud and clear-sky radiation processes as simulated by the Canadian regional climate model GEM. Mon Weather Rev 138:818–838

Pincus R, Hannay C, Klein SA, Xu KM, Hemler R (2005) Overlap assumptions for assumed probability distribution function cloud schemes in large-scale models. J Geophys Res 110, D15S09. doi:10.1029/2004JD005100

Platnick S, King MD, Ackerman SA, Menzel WP, Baum BA, Riedi JC, Frey RA (2003) The MODIS cloud products: algorithms and examples from Terra. IEEE T Geosci Remote 41:459–473

Platt CM et al (1994) The experimental cloud lidar pilot study (ECLIPS) for cloud–radiation research. Bull Am Meteor Soc 75:1635–1654

Räisänen P, Barker HW, Khairoutdinov M, Li J, Randall DA (2004) Stochastic generation of subgrid-scale cloudy columns for largescale models. Q J R Meteorol Soc 130:2047–2067

Randall DA et al (2007) The physical science basis contribution of working group I to the fourth assessment report of the intergovernmental panel on climate change. Cambridge University, Cambridge

Rosenkranz PW (2003) Rapid radiative transfer model for AMSU/HSB channels. IEEE T Geosci Remote. doi:10.1109/TGRS.2002.808323

Rossow WB, Schiffer RA (1999) Advances in understanding clouds from ISCCP. Bull Am Meteor Soc 80:2261–2287

Rossow WB, Zhang YC (1995) Calculation of surface and top of atmosphere radiative fluxes from physical quantities based on ISCCP data sets, 2. Validation and first results. J Geophys Res 100:1167–1197

Rossow WB, Gardner LC, Lacis AA (1989) Global seasonal cloud variations from satellite radiance measurements. Part I: sensitivity of analysis. J Clim 2:419–458

Sengupta M, Clothiaux EE, Ackerman TP (2004) Climatology of warm boundary layer clouds at the ARM SGP site and their comparison to models. J Clim 17:4760–4782

Shonk JKP, Hogan RJ, Edwards JM, Mace GG (2010) Effect of improving representation of horizontal and vertical cloud structure on the Earth's global radiation budget. Part I: review and parametrization. Q J R Meteorol Soc. doi:10.1002/qj.647

Slingo JM (1987) The development and verification of a cloud prediction scheme for the ECMWF model. Q J R Meteorol Soc. doi:10.1002/qj.49711347710

Stephens GL (2005) Cloud feedbacks in the climate system: a critical review. J Clim 18:237–273

Stephens GL et al (2002) The CloudSat mission and the a-train. Bull Am Meteor Soc 83:1771–1790

Stokes MG, Schwartz SE (1994) The atmospheric radiation measurement (ARM) program: programmatic background and design of the cloud and radiation test bed. Bull Am Meteor Soc 75:1201–1221

Sun R, Moorthi S, Xiao H, Mechoso CR (2010) Simulation of low clouds in the Southeast Pacific by the NCEP GFS: sensitivity to vertical mixing. Atmos Chem Phys. doi:10.5194/acp-10-12261-2010

Susskind J, Barnet CD, Blaisdell JM (2003) Retrieval of atmospheric and surface parameters from AIRS/AMSU/HSB data in the presence of clouds. IEEE T Geosci Remote 41:390–409

Susskind J, Barnet C, Blaisdell J, Iredell L, Keita F, Kouvaris L, Molnar G, Chahine M (2006) Accuracy of geophysical parameters derived from atmospheric infrared sounder/advanced microwave sounding unit as a function of fractional cloud cover. J Geophys Res. doi:10.1029/2005JD006272

Tian L, Curry JA (1989) Cloud overlap statistics. J Geophys Res 94:9925–9935

Tobin DC et al (2006) Atmospheric radiation measurement site atmospheric state best estimates for atmospheric infrared sounder temperature and water vapor retrieval validation. J Geophys Res. doi:10.1029/2005JD006103

Tiedtke M (1993) Representation of clouds in large-scale models. Mon Weather Rev 121:3040–3061

Tompkins A (2002) A prognostic parameterization for the subgrid-scale variability of water vapor and clouds in large-scale models and its use to diagnose cloud cover. J Atmos Sci 59:1917–1942

Walden VP, Roth WL, Stone RS, Halter B (2006) Radiometric validation of the atmospheric infrared sounder over the Antarctic Plateau. J. Geophys. Res. doi:10.1029/2005JD006357

Wang Z, Sassen K (2004) An improved cloud classification algorithm based on the SGP CART site observations. The Fourteenth ARM Science Team Meeting, Albuquerque, New Mexico. http://www.arm/gov/publications/proceedings.stm

Warren SG, Hahn CJ, London J (1985) Simultaneous occurrence of different cloud types. J Appl Meteorol Clim 24:658–667

Watanabe M, Emori S, Satoh M, Miura H (2009) A pdf-based hybrid prognostic cloud scheme for general circulation model. Clim Dyn. doi:10.1007/s00382-008-0489-0

Webb M, Senior C, Bony S, Morcrette JJ (2001) Combining ERBE and ISCCP data to assess clouds in the Hadley Centre, ECMWF and LMD atmospheric climate models. Clim Dyn 17:905–922

Wielicki BA, Cess RD, King MD, Randall DA, Harrison EF (1995) Mission to planet Earth: role of clouds and radiation in climate. Bull Am Meteor Soc 76:2125–2153

Wilson DR, Bushell AC, Kerr-Munslow AM, Price JD, Morcrette CJ (2008) PC2: a prognostic cloud fraction and condensation scheme. I: scheme description. Q J R Meteorol Soc 134:2093–2107

Xi B, Dong X, Minnis P, Khaiyer M (2010) A 10-year climatology of cloud fraction and vertical distribution derived from both surface and GOES observations over the DOE ARM SGP Site. J Geophys Res. doi:10.1029/2009JD012800

Xie SP et al (2007) A regional ocean–atmosphere model for eastern Pacific climate: toward reducing tropical biases. J Clim 20:1504–1522

Xu KM, Randall DA (1996) A semiempirical cloudiness parameterization for use in climate models. J Atmos Sci 53:3084–3102

Yang F, Pan HL, Krueger SK, Moorthi S, Lord SJ (2006) Evaluation of the NCEP global forecast system at the ARM SGP site. Mon Weather Rev 134:3668–3690

Yoo HL, Li Z (2012) Evaluation of cloud properties in the NOAA/NCEP global forecast system using multiple satellite products. Clim Dyn. doi:10.1007/s00382-012-1430-0

Zhang MH et al (2005) Comparing clouds and their seasonal variations in 10 atmospheric general circulation models with satellite measurements. J Geophys Res. doi:10.1029/2004JD005021